

Article

Removal of Model Aromatic Hydrocarbons from Aqueous Media with a Ferric Sulfate–Lime Softening Coagulant System

Deysi J. Venegas-García and Lee D. Wilson * 

Department of Chemistry, University of Saskatchewan, 110 Science Place, Thorvaldson Building, Saskatoon, SK S7N 5C9, Canada

* Correspondence: lee.wilson@usask.ca; Tel.: +1-306-966-2961

Abstract: The removal of model hydrocarbon oil systems (4-nitrophenol (PNP) and naphthalene) from laboratory water was evaluated using a ferric sulfate and a lime-softening coagulant system. This study addresses the availability of a methodology that documents the removal of BTEX related compounds and optimizes the ferric-based coagulant system in alkaline media. The Box–Behnken design with Response Surface Methodology enabled the optimization of the conditions for the removal (%) of the model compounds for the coagulation process. Three independent variables were considered: coagulant dosage (10–100 mg/L PNP and 30–100 mg/L naphthalene), lime dosage (50–200%), and initial pollutant concentration (1–35 mg/L PNP and 1–25 mg/L naphthalene). The response optimization showed a 28% removal of PNP at optimal conditions: 74.5 mg/L ferric sulfate, 136% lime dosage, and initial PNP concentration of 2 mg/L. The optimal conditions for naphthalene removal were 42 mg/L ferric sulfate, 50% lime dosage, and an initial concentration of naphthalene (16.3 mg/L) to obtain a 90% removal efficiency. The coagulation process was modeled by adsorption isotherms (Langmuir for PNP; Freundlich for Naphthalene). The surface properties of flocs were investigated with pH_{pzc} , solid-state UV absorbance spectra, and optical microscopy to gain insight into the role of adsorption in the ferric coagulation process.

Keywords: oil-spill; hydrocarbon model; coagulation; lime-softening; ferric sulfate; adsorption isotherms; UV–VIS spectroscopy



Citation: Venegas-García, D.J.; Wilson, L.D. Removal of Model Aromatic Hydrocarbons from Aqueous Media with a Ferric Sulfate–Lime Softening Coagulant System. *Surfaces* **2022**, *5*, 413–428. <https://doi.org/10.3390/surfaces5040030>

Academic Editor: Gaetano Granozzi

Received: 1 September 2022

Accepted: 16 September 2022

Published: 22 September 2022

Publisher's Note: MDPI stays neutral with regard to jurisdictional claims in published maps and institutional affiliations.



Copyright: © 2022 by the authors. Licensee MDPI, Basel, Switzerland. This article is an open access article distributed under the terms and conditions of the Creative Commons Attribution (CC BY) license (<https://creativecommons.org/licenses/by/4.0/>).

1. Introduction

The accidental or deliberate release of crude liquid petroleum oil and other derived oils into water is termed as an oil spill [1,2]. Crude oil spill disasters are a serious environmental hazard that cause widespread negative environmental and economic impacts. The accidental leakage of crude oil from transport tanks, pipelines, drilling platforms and rigs, and oil wells are known to occur during the extraction and transportation of oil through waterways [3]. Petroleum is a complex mixture containing hundreds of organic compounds whose composition depend on the source materials, formation conditions, and migration to and accumulation in reservoirs [4,5]. Serious physical and mental health effects [6,7] can be caused by the various polyaromatic hydrocarbons (PAHs) [8–11], petroleum hydrocarbons (PHCs) [12,13], volatile organic compounds (VOCs) [14,15], and other combustible products in petroleum. Polar substituted arenes (e.g., halogen and nitro groups) also have variable persistence, toxicity, and solubility in water [16–18].

Efficient decontamination and immediate clean-up to remove the oily slick layers over the water surface is critical for safeguarding the environment and aquatic biota [19,20]. Currently, various methods have been developed for highly polluted oilfield wastewaters or petroleum refinery wastewaters, such as demulsification, coagulation, adsorption, biodegradation, electrochemistry, and oxidation, as well as their combined processes [21]. Among these, coagulation processes offer an economical method that has been extensively applied due to its low infrastructure requirements, facile operation, and pollutant removal

efficiency [22]. Metal salts such as ferric chloride [23], ferric sulfate [24], aluminum sulfate [25], and polyaluminium chloride [26] are widely used coagulants that display a good efficiency for removal of hydrocarbon pollutants [27]. The metal salt hydrates and hydrolysis products (monomer/polymer species and solid precipitates) can act on the pollutant species with three main mechanisms: charge neutralization, sweep flocculation, and adsorption bridging. Generally, the mechanisms of coagulation that employ metal-based coagulants are strongly dependent on the hydrolysis products of coagulants [28].

In conventional industrial water treatment at the municipal level, lime-softening is a traditional and low-cost method used to reduce the hardness of water. Lime (lime-softening) is added to hard water to increase the pH of water. In turn, bicarbonates transform into carbonates, where Ca^{2+} and Mg^{2+} are eliminated from the water in the form of CaCO_3 and $\text{Mg}(\text{OH})_2$ species [29], where such water softening is conceived for reducing the levels of calcium and magnesium ions. Coagulation along with lime-softening has been proven to be an effective combination during water treatment processes for the removal of colloidal particles [30].

The City of Saskatoon water treatment plant (WTP) has identified the need to develop a methodology that employs lime-softening with ferric sulfate as the coagulant for the removal of model compounds that resemble crude oil, such as benzene, toluene, ethylbenzene, and xylene (BTEX) [31]. To mitigate the risks associated with crude oil spills, WTPs wish to develop mitigation strategies to protect source water. The main objective of this study serves to address a key knowledge gap related to the development of a ferric sulfate coagulation methodology under alkaline conditions for the removal of model hydrocarbon pollutants. This research will contribute toward the optimization of an effective ferric coagulant-based water treatment technology under alkaline conditions. The results from this study will contribute to the design of a multi-barrier approach that will allow WTPs to implement a coagulation-based treatment process that will safeguard drinking water from accidental crude oil spillage into source water supplies. This study will address the existing knowledge gap concerning oil removal through the development of a method that employs ferric sulfate as a coagulant system under alkaline conditions. In cooperation with the City of Saskatoon WTP, this study will address the removal of model pollutants from water. We envisage that the results of this study will contribute to a future mitigation strategy to address the potential occurrence of accidental oil spills (crude oil) into source water that can be adopted by other WTPs globally.

2. Materials and Methods

2.1. Materials

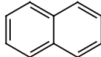
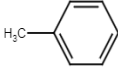
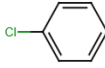
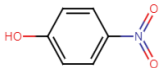
All of the chemicals were of analytical reagent (AR) grade. 4-nitrophenol, 99%, was obtained from Alfa Aesar (Tewksbury, MA, USA). Naphthalene (99.7%) was acquired from Mallinckrodt Pharmaceuticals (Blanchardstown, Dublin, Ireland). Potassium phosphate dibasic and potassium phosphate monobasic were purchased from Fisher Scientific (New York, NY, USA). Calcium carbonate (99%) was obtained from BDH Chemicals (Mississauga, ON, Canada). Benzene (99%), toluene (99.5%), and chlorobenzene (99.5%) were obtained from Sigma-Aldrich (Oakville, ON, Canada). All of the stock solutions were prepared using 18 M Ω cm Millipore, unless specified otherwise. Ferric sulfate (60% *w/v*) and lime (10% *w/v*) solutions were obtained from the City of Saskatoon Water Treatment Plant (Saskatoon, SK, Canada).

2.2. Model Selection

Several model compounds were initially selected (benzene, toluene, chlorobenzene, 4-nitrophenol, and naphthalene) for this study. In order to quantify the initial and final concentration for each of the “model” compounds, calibration curves were obtained for each, using UV–VIS spectroscopy. The boundary conditions of the concentration for the calibration range was based on an internal report [32] that estimated the total residual hydrocarbon level expected in the source water after an oil spill (ca. 10–20 mg/L). Based on

the residual oil estimated from this report, the maximum concentration range within the water column was estimated to be 10% (1–2 mg/L) of the oil concentration (ca. 10–20 mg/L). Thus, the range of concentration for the calibration curves and the coagulation trial experiments varied between 0.5 to 55 mg/L. Table 1 shows some selected properties for the model compounds examined in this study, which include selected physicochemical properties, as described above, including the wavelength for the maximum absorbance (λ_{\max}) for analytical detection.

Table 1. Summary of the physical properties for the model organic compounds *.

Properties	Naphthalene	Toluene	Benzene	Chlorobenzene	4-Nitrophenol
Chemical structure					
Chemical formula	C ₁₀ H ₈	C ₇ H ₈	C ₆ H ₆	C ₆ H ₅ Cl	C ₆ H ₅ NO ₃
Molecular weight (g/mol)	128.1	92.1	78.1	112.5	139.1
Water solubility (g/L)	0.0316	0.52	1.7	0.49	16
Vapor pressure 25 °C (mm Hg)	0.087	28.4	96	11	2.40 × 10 ⁻⁵
λ_{\max} (nm)	220	262	254	264	400

* Data was obtained from Mohammadi et al., 2020 [7].

Solutions for the model pollutant were analyzed by UV–Vis spectroscopy using a double beam Varian Cary-6000i (Santa Clara, CA, USA) spectrophotometer with a 3 mL quartz cuvette and 10 mm path length.

2.3. Coagulation Process

The coagulation was performed using a program-controlled conventional jar test apparatus with six 2 L jars and stirrers. Approximately 1 L of simulated polluted water was added to the jar test setup. For the laboratory water samples, a simulation of hardness was carried out with the addition of CaCO₃. An aliquot of the simulated polluted water solution was sampled to measure the initial pollutant concentration. The coagulation experiment was carried out by adapting the procedure described by Agbovi and Wilson, [33]. In brief, a predetermined amount of lime solution was added to the solution, which was mixed for 20 min, where the coagulant was then added, followed by rapid stirring for 3 min at 295 rpm. Thereafter, the stirring rate was reduced to 25 rpm for 20 min. The stirring was stopped to allow the sample to settle overnight, where a 10 mL sample was centrifuged at 500 rpm for 30 min. The supernatant was analyzed through the measurement of the Ultraviolet–visible (UV–VIS) spectrum at variable wavelengths. PNP was buffered in order to estimate the concentration at pH 7. Experiments were performed in duplicate, and the average values were reported. The removal efficiency (*RE*; %) and the adsorption capacity ($\text{mg}\cdot\text{g}^{-1}$) were calculated by Equations (1) and (2), respectively.

$$RE \% = \frac{C_o - C_e}{C_o} \times 100 \quad (1)$$

$$q_e = \frac{(C_o - C_e) \times V}{m} \quad (2)$$

Here, q_e is the adsorption of the pollutant onto the floc material generated after the coagulation process. C_o and C_e are the initial and equilibrium pollutant concentrations (mg/L), V is the volume (L), and m is the weight (g) of the metal salt coagulant system.

2.4. Box–Behnken Experimental Design

The Box–Behnken experimental design method was used to determine the effects of major operating variables on pollutant removal and to find the combination of variables that resulted in maximum removal efficiency. The Box–Behnken design (BBD) is a response

surface methodology that is a collection of mathematical and statistical techniques that are useful for the modelling and analysis of data, wherein a response of interest is influenced by several variables and the objective is to optimize this response [34]. Preliminary experiments indicate that three important operating parameters play a key role in pollutant removal in the coagulation process: coagulant dosage (ferric sulfate; A), lime dosage (B), and the initial pollutant concentration (C). These variables were chosen as the independent variables and were designated as A (1–100 mg/L), B (50–200% relative to the ferric sulfate concentration), and C (1–35 mg/L), respectively.

When correlating the pollutant removal efficiency (Y) with other independent variables (A, B, and C), a response surface function was utilized (cf. Equation (3)). Where Y acts as the predicted response surface function; b_0 is the model constant; b_1 , b_2 , and b_3 are the linear coefficients; b_{12} , b_{13} , and b_{23} are the cross product coefficients; and b_{11} , b_{22} , and b_{33} are the quadratic coefficients in Equation (3). The response function coefficients were determined by regression analysis of the experimental data and the Minitab 19 DOE regression program.

$$Y = b_0 + b_1A + b_2B + b_3C + b_{12}AB + b_{13}AC + b_{23}BC + b_{11}A^2 + b_{22}B^2 + b_{33}C^2 \quad (3)$$

The BBD for the removal of the selected models was carried out with three factors (ferric sulfate, lime, and an initial pollutant concentration) and at three levels (−1, 0, 1). Table 2 shows the levels for each of the factors for this experiment. The complete BBD description is presented in Table S1 (Supplementary Materials). Preliminary results indicate that the water hardness could have a significant effect on the removal of the model pollutants. Thus, the content of carbonate in all of the model systems was adjusted to 125 mg/L as CaCO_3 .

Table 2. Levels of each factor for Box–Behnken analysis for the removal of pollutants.

Model	Independent Factors								
	A			B			C		
	Ferric Sulfate (mg L ^{−1})			Lime (%) ¹			Pollutant (mg L ^{−1})		
	−1	0	1	−1	0	1	−1	0	1
PNP	10	55	100	50	125	200	1	18	35
Naphthalene	30	65	100	50	125	200	1	18	25

¹ The lime dosage is based on a relative (%) concentration to that of ferric sulfate.

2.5. Adsorption Isotherms

Adsorption isotherms provide insight concerning the interaction between adsorbates and adsorbents at optimal conditions to elucidate the coagulation mechanism. The Langmuir and Freundlich isotherm models are the most frequently used to describe adsorption during a coagulation processes of colloidal particles [35].

The Langmuir adsorption isotherm model is based on the assumption that adsorption occurs at specific homogeneous sites with the adsorbent, and is described by Equation (4).

$$q_e = \frac{K_1 q_m C_e}{1 + K_1 C_e} \quad (4)$$

q_m (mg·g^{−1}) is the monolayer adsorption of pollutant per unit mass of ferric sulfate–lime adsorbent, where q_e is the amount of adsorbed pollutant (mg·g^{−1}). K_1 (L·g^{−1}) is the equilibrium adsorption constant, which is related to the affinity of the binding sites and is related to a dimensionless constant called the separation factor or equilibrium variable, R_l , according to Equation (5). The adsorption process can be divided into four categories

based on the value of R_l : irreversible ($R_l = 0$), favorable ($0 < R_l < 1$), linear ($R_l = 1$), and unfavorable ($R_l > 1$) [36].

$$R_l = \frac{1}{1 + K_1 C_0} \quad (5)$$

The Freundlich isotherm model accounts for multilayer sorption by assuming that the adsorbent has a heterogeneous surface with non-uniform distribution of the sorption sites, as described by Equation (6).

$$q_e = K_f C_e^{1/n} \quad (6)$$

K_f is the Freundlich isotherm constant, which relates to the adsorption capacity, and n is a dimensionless constant. The empirical exponent variable gives valuable information on the shape of the isotherm, where the adsorption process may be classified as unfavorable ($1/n > 1$), favorable ($1/n < 1$), or irreversible ($1/n = 0$) [37].

Adsorption isotherms were conducted in 8-dram vials with 25 mL of PNP with a concentration from 0.1 to 3 mg/L and for naphthalene from 1 to 20 mg/L. Ferric sulfate, lime, and calcium carbonate were added at optimal conditions for each pollutant. Vials were placed on an orbital shaker and were mixed at 295 rpm for 3 min, followed by 20 min at 25 rpm. After the adsorption process, samples were treated as described in Section 2.2. The adsorption capacities were determined according to Equation (2).

2.6. pH at Point-of-Zero-Charge

The point-of-zero-charge (pH_{pzc}) of materials was determined according to Kong and Wilson [38]. A stock solution of NaCl (0.01 M) was prepared and 20 mL portions were transferred into eight vials (8-dram). The solution pH conditions of the samples were adjusted between pH 3 to 10 using aqueous NaOH or HCl solutions. The sorbent materials (45 mg) were added to each solution and were allowed to equilibrate for 48 h before the final pH was recorded. The pH_{pzc} was estimated by plotting the final pH against the initial pH, and the point of intersection of the resulting null pH refers to the point zero charge, pH_{pzc} .

2.7. Solid State UV–VIS Spectroscopy

Floc samples were layered onto glass microscope slides and allowed to dry under ambient conditions prior to analysis of the spectra in the solid state with a Varian Cary-6000i (Santa Clara, CA, USA) spectrophotometer. The spectra were obtained in a solid sample holder for naphthalene ($\lambda = 200\text{--}340$ nm) and PNP ($\lambda = 200\text{--}800$ nm), ferric sulphate flocs, and ferric sulfate flocs that contain PNP and naphthalene, respectively.

2.8. Optical Microscopy

Small samples of isolated wet flocs were dropped onto a microscope slide for analysis using optical microscopy. In order to avoid alteration of the floc structure, because of compression, no cover slips were used. Digital images of the flocs were captured on a Renishaw InVia Reflex Raman microscope (Renishaw plc, New Mills, UK) with $5\times$ magnification.

3. Results

Upon consideration of various physicochemical properties (cf. Table 1) that were used to select suitable model hydrocarbon oils, PNP and naphthalene were chosen as the model compounds for this study. Key factors include the reliability of calibration curves, molar absorptivity, solubility in water, and minimal vapor pressure to avoid evaporative losses during the coagulation treatment process. The removal efficiency for the model hydrocarbon systems was studied in the laboratory at optimized conditions through the Box–Behnken experimental design. Optical microscopy, UV–VIS spectroscopy, and pH_{pzc} and used to characterize the surface properties of the isolated flocs, where the results are outlined in the sections below.

3.1. Model Selection

Figure 1a presents the spectra (200 nm to 230 nm) where the UV absorption band of naphthalene is visible. Naphthalene (0.5–10 mg/L) showed a maximum absorption at 220 nm. Toluene covers a wider concentration range from 0.5 to 50 mg/L. The spectrum for toluene is presented in Figure 1b (230 nm to 280 nm), where the absorption bands are visible with a maximum absorption at 262 nm. The spectra for benzene (230 nm to 280 nm) is presented in Figure 1c. Characteristic absorption bands for benzene (1–35 mg/L) within this spectral range are clearly visible, with a maximum absorbance at $\lambda = 254$ nm. The chlorobenzene concentration was wide-ranging from 0.1 to 55 mg/L, where the spectrum for chlorobenzene is shown in Figure 1d ($\lambda = 230$ nm to 280 nm), which shows a maximum absorption at $\lambda = 264$ nm. 4-nitrophenol shows an absorption maximum at $\lambda = 400$ nm to enable the construction of a calibration curve (Figure 1e). The R-adj coefficients for each of the model systems were 0.999 (naphthalene), 0.998 (toluene), 0.993 (benzene), 0.997 (chlorobenzene), and 0.999 (PNP). These values showed a good linear correlation.

3.2. Box–Behnken Analysis (BBD)

Based on the calibration curve results presented for toluene, benzene, and chlorobenzene over the concentrations range outlined in the final report, this [32] indicated low absorbance values (below 0.08 absorbance units). As these values are below the limit of quantification (LOQ) [39], BBD was carried out only for naphthalene and PNP, in line with their favorable water solubility and lower vapor pressure (cf. Table 1).

Table 3 shows *p*-values for each factor and coefficients for the model pollutant removal. Equation (3) can be used for modelling the pollutant removal within the range established for each factor. For PNP, ferric sulfate, initial PNP concentration, and lime dosage are significant factors over PNP removal due to the lower *p*-value (<0.05). Furthermore, the squared interaction for each of the factors showed significant effects. The initial naphthalene concentration and lime dosage were significant factors over naphthalene removal due to the *p*-value lower than 0.05. Furthermore, the squared interaction for naphthalene revealed a significant effect. ANOVA analysis is presented in Table S2 for PNP and Table S3 for naphthalene in the Supplementary Materials.

Table 3. Coded coefficients for the removal of model pollutants and *p*-values.

Model Term	PNP		Naphthalene	
	Coeff.	<i>p</i> -Value	Coeff.	<i>p</i> -Value
Constant	17.596	0.000	89.000	0.000
Ferric sulfate	−7.879	0.000	5.563	0.000
Lime	1.183	0.043	−0.563	0.138
Pollutant	1.671	0.006	−1.000	0.012
Ferric sulfate × ferric sulfate	2.791	0.004	−9.500	0.000
Lime × lime	−1.746	0.042	−0.500	0.362
Pollutant × pollutant	−7.221	0.000	−0.625	0.257
Ferric sulfate × lime	−0.258	0.749	1.000	0.066
Ferric sulfate × pollutant	−0.283	0.725	−0.125	0.811
Lime × pollutant	0.400	0.610	0.375	0.475

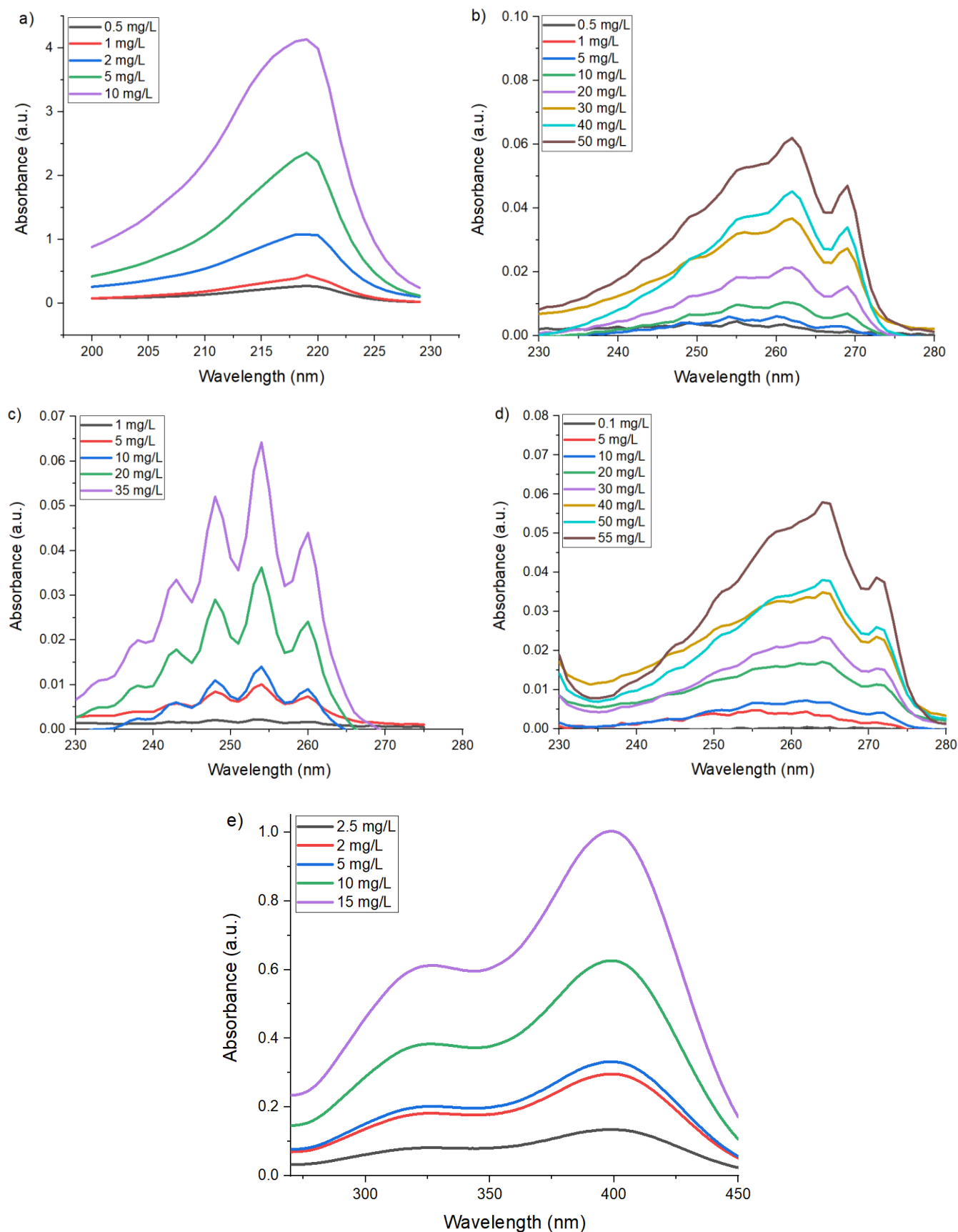


Figure 1. UV-VIS spectra for model compounds in water at variable concentration: (a) naphthalene, (b) toluene, (c) benzene, (d) chlorobenzene, and (e) PNP.

The effect of the main factors for pollutant removal is presented in Figure 2. The removal of PNP decreases as the initial concentration of PNP increases from 1 to 35 mg/L. Increasing the ferric sulfate concentration from 1 to 70 mg/L led to an increase in the removal to a maximum (18%) at 75 mg/L of ferric sulfate. Then, the removal underwent a decrease as the ferric sulfate concentration increased up to 100 mg/L. Lime dosage presented the highest removal (18%) when added at 136% relative to the ferric sulfate concentration, whereas the PNP removal decreased as the lime dosage increased up to 200% (Figure 2a). The response optimization showed a PNP removal of 28% achieved at optimal conditions: ferric sulfate (74.5 mg/L), lime dosage (136%) based on ferric sulfate concentration, and an initial concentration of PNP (2 mg/L). The effect of the main factors for naphthalene removal are presented in Figure 2b. For an initial concentration of naphthalene, its removal decreased as its concentration increased, where a maximum removal (90%) occurred at 16.3 mg/L naphthalene. Increasing the ferric sulfate concentration from 30 to 100 mg/L yielded a decreased removal with a maximum (88%) that occurred at 42 mg/L of ferric sulfate. Then, the removal decreased as the ferric sulfate level increased up to 100 mg/L. The lime dosage presented the highest removal (88%) when it was added at 50% (relative to the ferric sulfate concentration), while naphthalene removal decreased as the lime dosage increased up to 200%. The response optimization showed a naphthalene removal of 90% that could be achieved at optimal conditions: ferric sulfate (42 mg/L), lime dosage (50%) based on ferric sulfate concentration, and an initial concentration of naphthalene (16.3 mg/L).

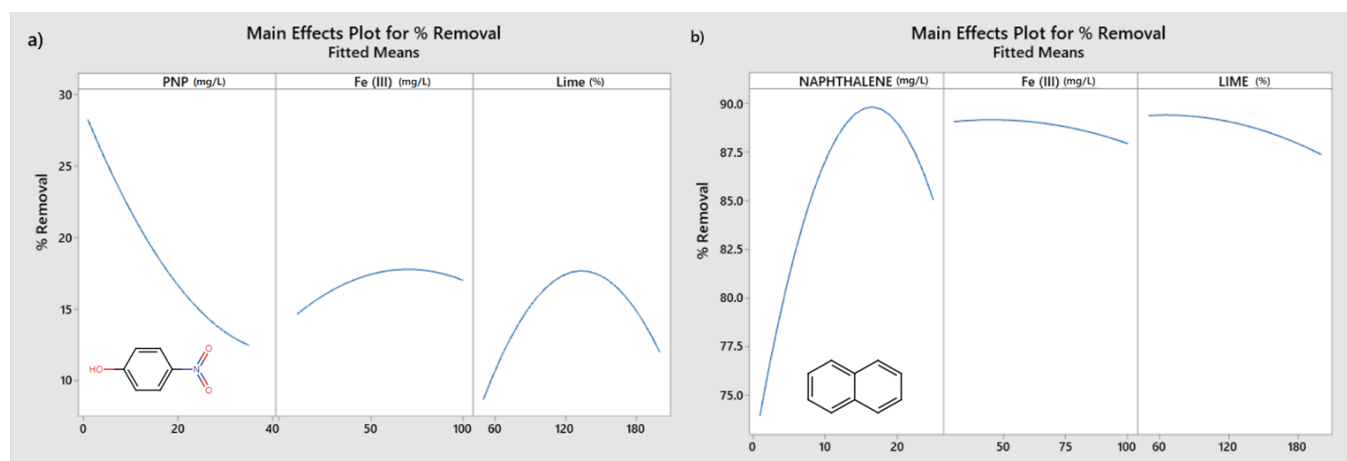


Figure 2. Main factors that govern model pollutant removal: (a) PNP and (b) naphthalene.

The contour plots herein describe how pollutant removal changes as a function of the ferric sulfate concentration, lime dosage, and initial pollutant concentration. As well, the contour plots show the removal through the combination of two factors, which allow for the third factor to be set at the middle value. The contour plots presented in Figure 3a, show the combinations for an initial PNP concentration and ferric sulfate concentration, with the lime dosage set at a middle value (125%) for the removal of PNP.

The removal of PNP for a lime dosage and PNP initial concentration with ferric sulfate set at the middle value (55 mg/L) is shown in Figure 3b. In Figure 3c, the removal of PNP is shown for variable lime and ferric sulfate dosage, where the initial concentration of PNP was fixed at 18 mg/L.

The combination of conditions for the naphthalene initial concentration and ferric sulfate dosage, with lime dose, was set at the middle value (125%), where the removal of naphthalene is presented in Figure 4a. Naphthalene removal for lime dosage and the naphthalene initial concentration with ferric sulfate was set at the middle value (55 mg/L), as shown in Figure 4b. The removal of naphthalene that considers lime and ferric sulfate dosage with the initial naphthalene concentration at 13 mg/L is presented in Figure 4c.

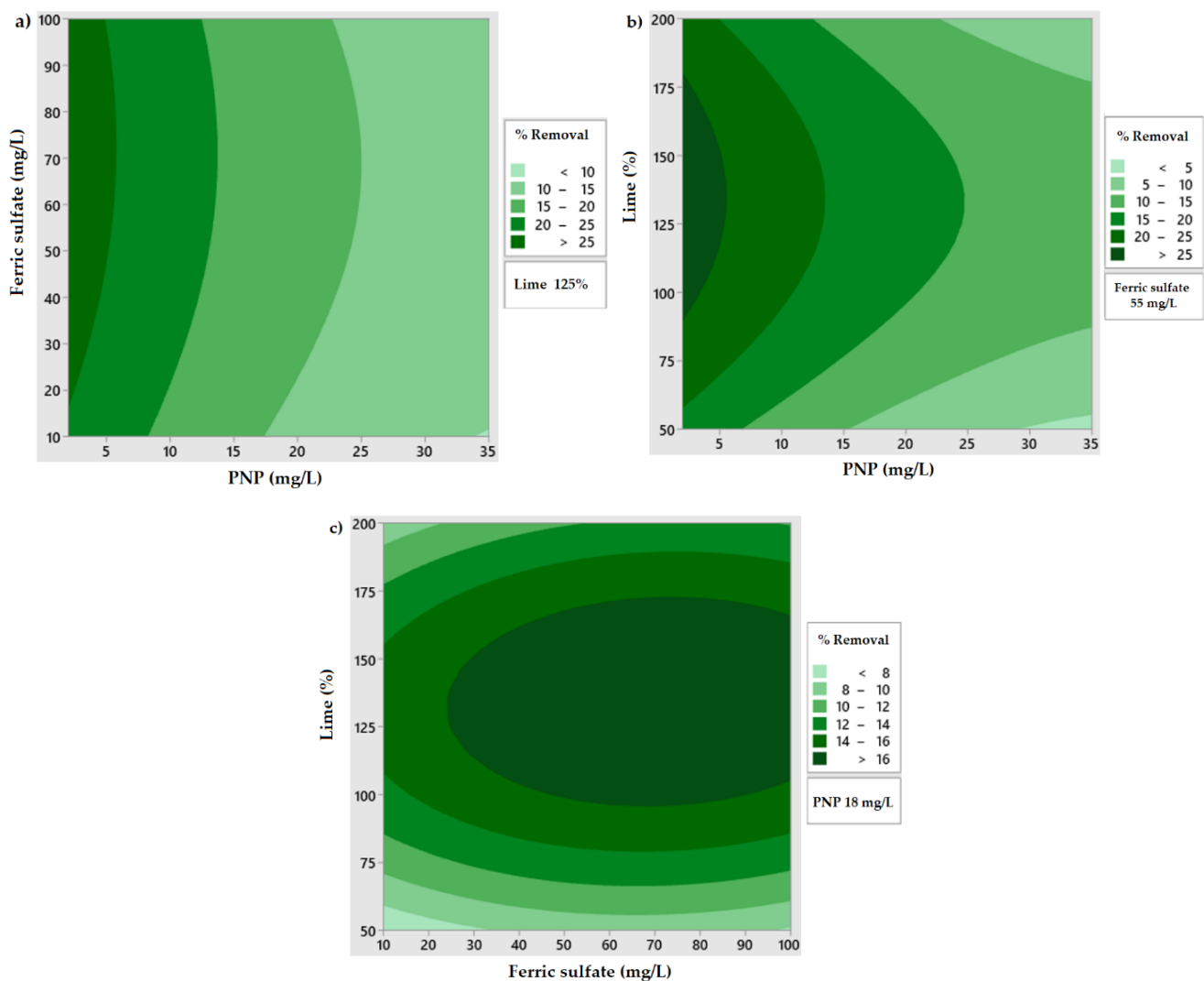


Figure 3. Contour plot for PNP removal (%; according to green shading) at variable conditions: (a) ferric sulfate (10–100 mg/L) and PNP initial concentration (1–35 mg/L); (b) PNP initial concentration (1–35 mg/L) and lime dosage (50–200%); and (c) ferric sulfate (10–100 mg/L) and lime dosage (50–200%).

3.3. Adsorption Isotherms

Figure 5 illustrates the adsorption isotherm profiles for the removal of PNP (Figure 5a) and naphthalene (Figure 5b) for the ferric sulfate–lime process. The fitted lines through the data represent the goodness-of-fit of the isotherm models employed herein, where the variables are listed in Table 4. Based on the tabular results, the removal of PNP and naphthalene by the ferric sulfate–lime system is well-described by the Langmuir ($R^2 = 0.970$) and Freundlich ($R^2 = 0.977$) models, respectively.

The dimensionless constant R_l obtained from the Langmuir model (0.583) indicates favorable adsorption of PNP. The monolayer adsorption capacity (q_m ; $\text{mg}\cdot\text{g}^{-1}$) for PNP at the optimized conditions was 17.4 ± 4.7 and the Langmuir adsorption constant, K_l , was 0.356 ± 0.19 . The values obtained from the Langmuir and Freundlich models are in agreement, and may be considered equally based on the goodness-of-fit and standard error of the isotherm results for the ferric sulfate–lime system.

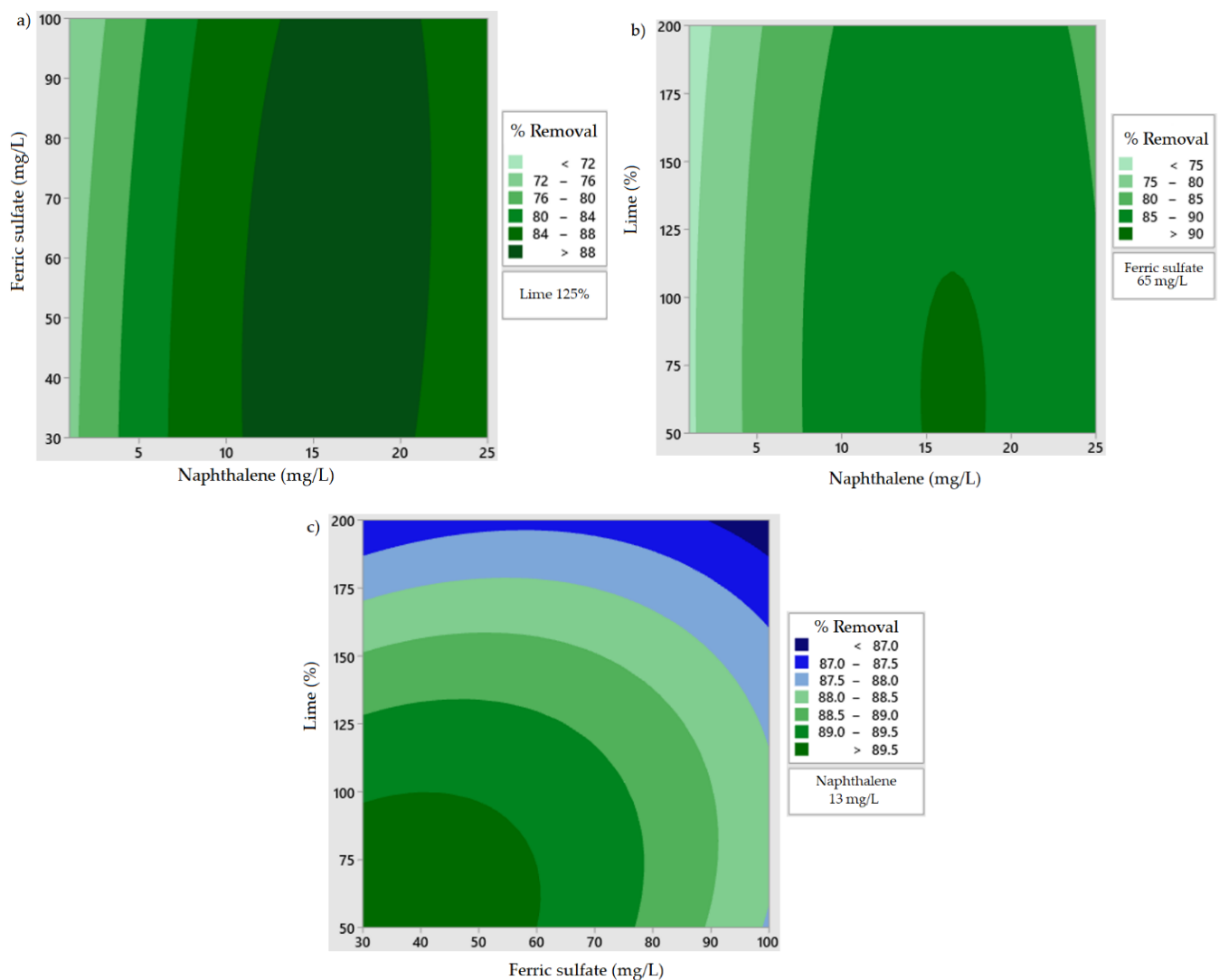


Figure 4. Contour plot for naphthalene removal (%; according to colour shading) at variable conditions: (a) ferric sulfate (30–100 mg/L) and naphthalene initial concentration (1–25 mg/L); (b) lime dosage (50–200%) and naphthalene initial concentration (1–25 mg/L); and (c) lime dosage (50–200%) and ferric sulfate (30–100 mg/L).

Table 4. Langmuir and Freundlich isotherm coefficients for the coagulation of PNP and naphthalene by ferric sulfate–lime system at 295 K.

		PNP		Naphthalene			
		Langmuir		Langmuir		Freundlich	
q_e	17.9 ± 5.83 ($\text{mg}\cdot\text{g}^{-1}$)	n	1.36 ± 0.24	q_e	779 ± 205 ($\text{mg}\cdot\text{g}^{-1}$)	n	1.14 ± 0.06
K_1	0.35 ± 0.19	K_f	4.50 ± 0.39	K_1	0.07 ± 0.02	K_f	52.9 ± 3.47
R^2	0.970	R^2	0.951	R^2	0.969	R^2	0.977
R_1	0.583			R_1	0.467		

In Table 4, the best-fit results for the adsorption isotherms of naphthalene are described by the Freundlich model, which is often used to describe the adsorption at heterogeneous surface sites and multilayer adsorption that may occur between naphthalene and ferric species. The n value ($1/n = 0.87$), presented in Table 4, indicate a favorable adsorption and heterogeneous surface sites, which concurs with the adsorption of naphthalene onto the floc surface in a coplanar to an orthogonal modality. In the present study, as n lies

between 1 and 10, which indicates the physical adsorption of naphthalene onto the ferric sulfate–lime floc system. A number of studies support that the adsorption process for naphthalene onto various adsorbents is favored by the Freundlich model, as compared with other isotherm models [40].

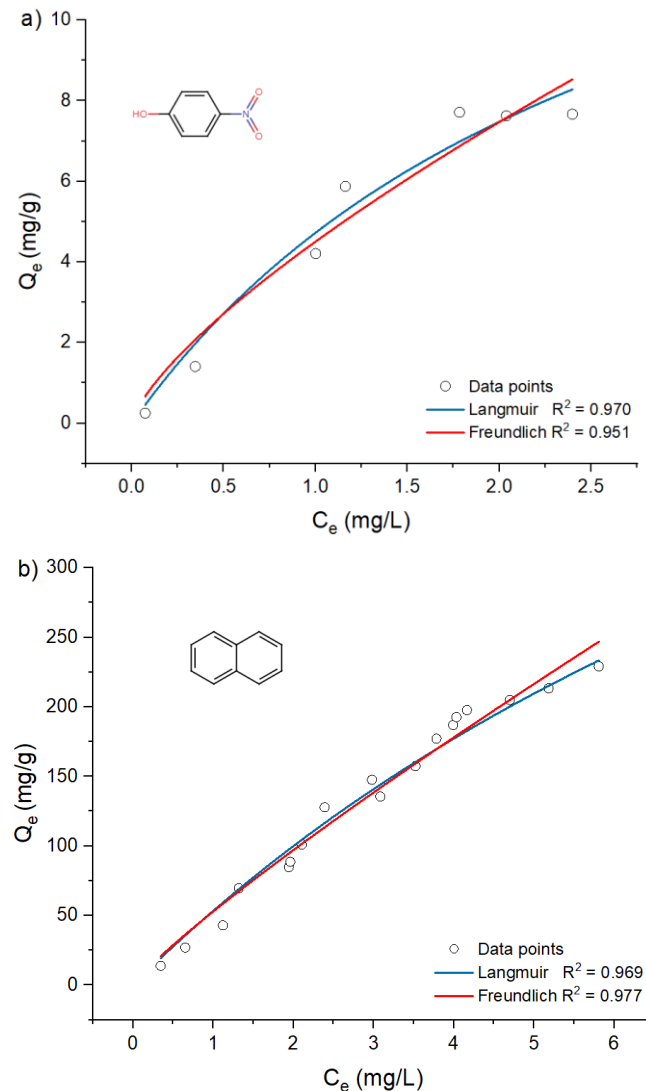


Figure 5. Adsorption isotherms of (a) PNP and (b) naphthalene by combined ferric sulfate–lime coagulation process at 295 K and optimized conditions.

3.4. Floc Surface Study

In order to study the mechanism for the coagulation process, ferric sulfate–lime flocs were isolated, washed, and air dried. Figure 6a shows the pH_{pzc} plot for the flocs formed by this system. The pH_{pzc} parameter indicates the pH where the net charge of a material is zero ($\text{pH} = 9.56$). The surface charge of the adsorbents is positive at a pH below the pH_{pzc} , where the adsorption of OH^- ions and other carbonate anion species may occur because the ζ -potential of the sorbent is positive overall. Meanwhile, the ζ -potential of the floc is negative when the solution pH lies above pH_{pzc} , where adsorption of the cation species mainly occurs due to favorable surface charge on the floc surface.

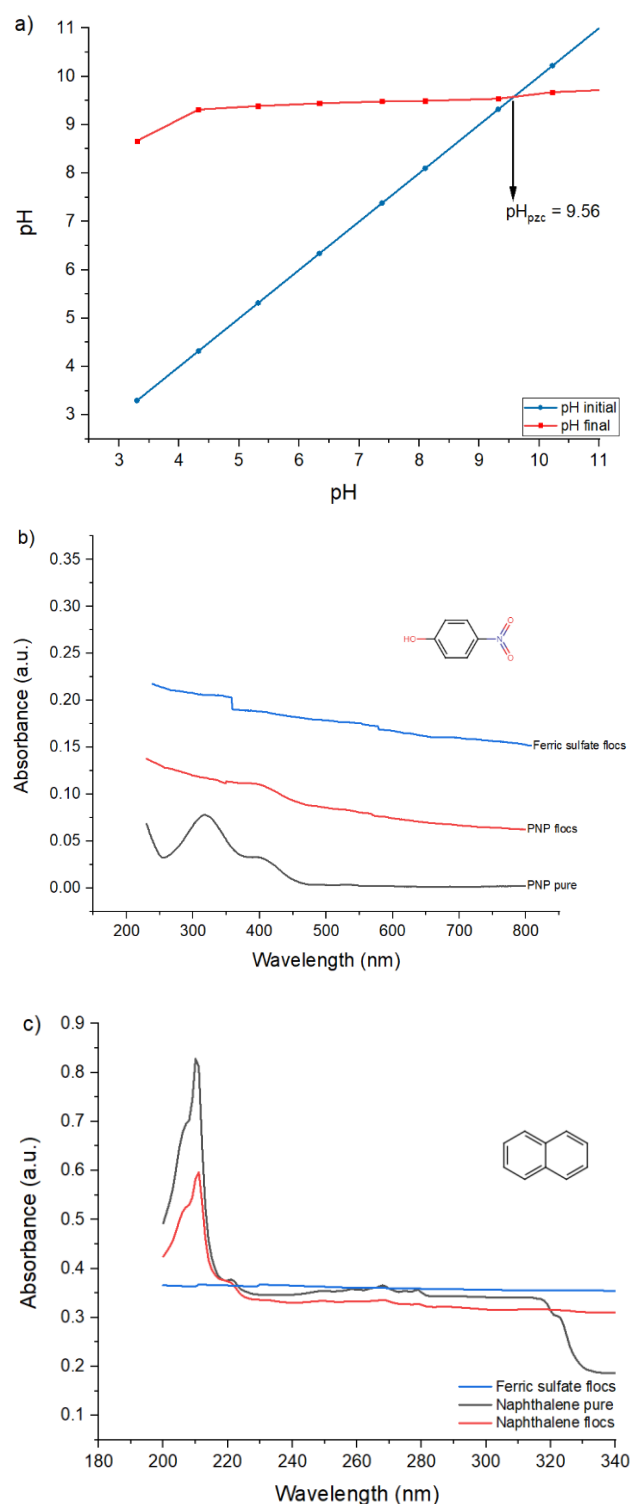


Figure 6. (a) pH_{pzc} for ferric flocs and solid UV-VIS spectra for (b) PNP (unbound and floc form) and (c) naphthalene (unbound and floc form), including isolated ferric sulfate flocs (without model pollutant).

Assuming that a negative surface charge prevails for the ferric sulfate flocs formed during coagulation with PNP at pH 11.5, and considering divalent ions, such as Ca^{2+} are present in water, the proposed mechanism is ion binding. Ion binding can occur between anionic colloids and negatively charged surfaces when there are enough divalent ions present in water, where such cations may serve as bridging units between the PNP and the

floc surface (cf. graphical abstract). The coagulation mechanism proposed for naphthalene ($\text{pH} = 10.5$) is likely to follow the ion bridging and favorable π -anion interaction.

After the coagulation process for PNP and naphthalene, the flocs were isolated and washed with Millipore water, and then air-dried over a quartz slide. Figure 6b shows the UV spectra for pure PNP (black) that present absorption bands at 317 and 400 nm, characteristic features for the non-ionized and ionized forms of PNP, respectively. These two states can co-exist when the pH is near to the pK_a (7.16) of PNP [41]. The slightly greater adsorption band at 400 nm for PNP flocs (red) shows that PNP is present in ionized form in the flocs. This trend confirms the ion binding mechanism between the anionic PNP with the negatively charged ferric species and the divalent cations. The presence of naphthalene (Figure 6c) on the surface of the flocs is also supported by the observed adsorption band at 220 nm (red).

Figure 7 presents the optical images of the flocs with a magnified ($5\times$) view. Figure 7a shows the flocs for PNP where some general morphological features include their large size and irregular shape. The microscopy image for the naphthalene flocs (Figure 7b) present variable floc sizes with a denser appearance, in comparison with the flocs noted for PNP.

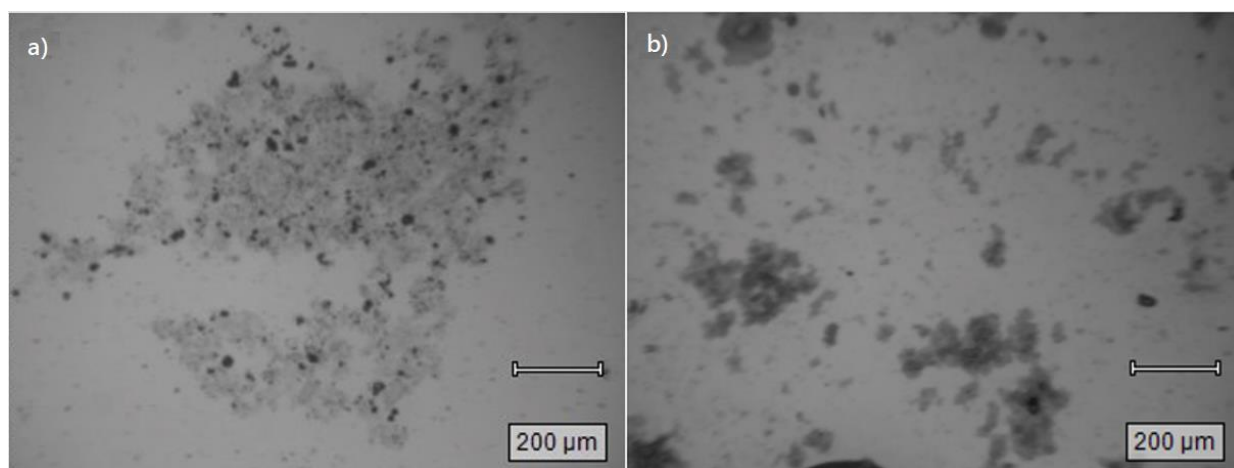


Figure 7. Optical microscopy images ($5\times$) for (a) PNP and (b) naphthalene isolated flocs.

4. Conclusions

To address the availability of limited published work for the removal of BTEX-related systems using ferric coagulation technology, this study focused on the design of an optimized methodology that employed a ferric sulfate coagulant system under lime-softening conditions. Two types of hydrocarbon oil-based model compounds were studied as representative pollutants: 4-nitrophenol (PNP) and naphthalene. PNP and naphthalene were quantified using UV–VIS spectrophotometry, and these model compounds possess favorable physical properties such as lower evaporative loss, in contrast with conventional model BTEX systems (cf. Table 1). A Box–Behnken statistical design was used to determine the experimental effects of coagulant dosage, lime dosage, and initial pollutant concentration for PNP and naphthalene removal efficiency. The coagulation removal efficiency (RE ; %) of the ferric sulfate–lime softening system was investigated using variable pollutant levels from 1 to 35 mg/L, based on their water solubility. The Box–Behnken Design and statistical experiment with the response surface methodology were effective for determining the optimal conditions for the removal of PNP (74.5 mg/L) and naphthalene (42 mg/L) through the ferric sulfate coagulation process. The optimum lime dosage for maximum PNP and naphthalene removal were found to be 136% and 50%, based on the ferric sulfate concentration, in that order. The initial PNP concentration was 2 mg/L at the optimized level, whereas the concentration for naphthalene was 16.3 mg/L, which concurs with their relative charge state and water solubility profiles (cf. Table 1), especially at alkaline conditions.

The Langmuir model described the isotherm results for PNP, whereas the Freundlich model accounted for the naphthalene adsorptive removal. The pH_{pzc} for flocs formed with the ferric sulfate–lime system provide insight into the mechanism for the coagulation process, with carbonate ion binding at the ferric floc surface sites as the main mechanism. The presence of PNP and naphthalene at the floc surface was corroborated by solid state UV spectroscopy and imaging of the flocs by optical microscopy. The application of the ferric sulfate coagulant system with lime-softening for the removal of PNP and naphthalene offers a potential remediation technique that can be deployed to mitigate the effects of crude oil spills. Ultimately, the ability to achieve complete removal of crude oil components will depend on the presence of competitor pollutant species in the source water and the effective solubility of the oil species, according to the conditions of the ferric sulfate–lime water process. Further studies are underway to establish greater removal efficiency, which build upon enhanced floc formation and the adsorption stability of BTEX model systems onto the floc surface sites for this process.

Supplementary Materials: The following supporting information can be downloaded at: <https://www.mdpi.com/article/10.3390/surfaces5040030/s1>, Table S1: Box–Behnken experimental design for the removal of pollutants, Table S2: Analysis of variance for PNP, Table S3: Analysis of variance for naphthalene.

Author Contributions: Conceptualization, L.D.W.; methodology, D.J.V.-G.; software, D.J.V.-G.; validation, D.J.V.-G. and L.D.W.; formal analysis, D.J.V.-G.; investigation, D.J.V.-G.; resources, L.D.W.; data curation, D.J.V.-G.; writing—original draft preparation, D.J.V.-G.; writing—review and editing, D.J.V.-G. and L.D.W.; visualization, D.J.V.-G.; supervision, L.D.W.; project administration, L.D.W.; funding acquisition, L.D.W. All authors have read and agreed to the published version of the manuscript.

Funding: This research was funded by The University of Saskatchewan and the City of Saskatoon, through the Research Junction Development Grant (Internal ID 354979) for the project titled, “Addressing water security for the City of Saskatoon Water Treatment Plant—Evaluating the efficacy of a coagulant-flocculant system for addressing oil-based waterborne contaminants from oil spills”. The APC was funded by the Surfaces Editorial office of MDPI.

Institutional Review Board Statement: Not applicable.

Informed Consent Statement: Not applicable.

Data Availability Statement: Not applicable here.

Acknowledgments: The authors wish to acknowledge the support for this project through a Research Junction grant provided by the City of Saskatoon and the University of Saskatchewan. The technical support provided by the Heng Yang and Mostafa Solgi, along with helpful discussions with Rob St. Pierre and Sunday Ibok, are gratefully acknowledged.

Conflicts of Interest: The authors declare no conflict of interest.

References

1. Popovici, D.R.; Neagu, M.; Dutescu-Vasile, C.M.; Bombos, D.; Mihai, S.; Oprescu, E.-E. Adsorption of *p*-Nitrophenol onto Activated Carbon Prepared from Fir Sawdust: Isotherm Studies and Error Analysis. *React. Kinet. Mech. Catal.* **2021**, *133*, 483–500. [[CrossRef](#)]
2. Singh, H.; Bhardwaj, N.; Arya, S.K.; Khatri, M. Environmental Impacts of Oil Spills and Their Remediation by Magnetic Nanomaterials. *Environ. Nanotechnol. Monit. Manag.* **2020**, *14*, 100305. [[CrossRef](#)]
3. Okoro, O.; Papineau, I.; Sollicec, M.; Fradette, L.; Barbeau, B. Performance of Conventional Drinking Water Treatment Following Dispersant Remediation of an Oil Spill in Surface Water. *Sci. Total Environ.* **2021**, *801*, 149583. [[CrossRef](#)] [[PubMed](#)]
4. Ren, G.; Han, H.; Wang, Y.; Liu, S.; Zhao, J.; Meng, X.; Li, Z. Recent Advances of Photocatalytic Application in Water Treatment: A Review. *Nanomaterials* **2021**, *11*, 1804. [[CrossRef](#)]
5. Okoro, O.; Lompe, K.; Papineau, I.; Sollicec, M.; Fradette, L.; Barbeau, B. Simultaneous Powdered Activated Carbon and Coagulant Injection during Ballasted Flocculation for Trace Benzene Removal from Diesel and Gasoline-Contaminated Surface Waters. *J. Water Process Eng.* **2021**, *40*, 101846. [[CrossRef](#)]

6. Gaurav, G.K.; Mehmood, T.; Kumar, M.; Cheng, L.; Sathishkumar, K.; Kumar, A.; Yadav, D. Review on Polycyclic Aromatic Hydrocarbons (PAHs) Migration from Wastewater. *J. Contam. Hydrol.* **2021**, *236*, 103715. [[CrossRef](#)]
7. Mohammadi, L.; Rahdar, A.; Bazrafshan, E.; Dahmardeh, H.; Susan, M.A.B.H.; Kyzas, G.Z. Petroleum Hydrocarbon Removal from Wastewaters: A Review. *Processes* **2020**, *8*, 447. [[CrossRef](#)]
8. Mansouri, E.; Yousefi, V.; Ebrahimi, V.; Eyvazi, S.; Hejazi, M.S.; Mahdavi, M.; Mesbahi, A.; Tarhriz, V. Overview of Ultraviolet-based Methods Used in Polycyclic Aromatic Hydrocarbons Analysis and Measurement. *Sep. Sci. PLUS* **2020**, *3*, 112–120. [[CrossRef](#)]
9. Travkin, V.M.; Solyanikova, I.P. Salicylate or Phthalate: The Main Intermediates in the Bacterial Degradation of Naphthalene. *Processes* **2021**, *9*, 1862. [[CrossRef](#)]
10. Gushchin, A.A.; Grinevich, V.I.; Izvekova, T.V.; Kvitkova, E.Y.; Sulaeva, O.Y.; Baburina, E.M.; Rybkin, V.V. Water Purification to Remove Naphthalene by Treatment with Dielectric-Barrier Discharge in Oxygen. *High Energy Chem.* **2022**, *56*, 208–212. [[CrossRef](#)]
11. Eldos, H.I.; Zouari, N.; Saeed, S.; Al-Ghouti, M.A. Recent Advances in the Treatment of PAHs in the Environment: Application of Nanomaterial-Based Technologies. *Arab. J. Chem.* **2022**, *15*, 103918. [[CrossRef](#)]
12. Negi, H.; Verma, P.; Singh, R.K. A Comprehensive Review on the Applications of Functionalized Chitosan in Petroleum Industry. *Carbohydr. Polym.* **2021**, *266*, 118125. [[CrossRef](#)] [[PubMed](#)]
13. Elmobarak, W.F.; Hameed, B.H.; Almomani, F.; Abdullah, A.Z. A Review on the Treatment of Petroleum Refinery Wastewater Using Advanced Oxidation Processes. *Catalysts* **2021**, *11*, 782. [[CrossRef](#)]
14. Dehghani, M.; Mohammadpour, A.; Abbasi, A.; Rostami, I.; Gharehchahi, E.; Derakhshan, Z.; Ferrante, M.; Conti, G.O. Health Risks of Inhalation Exposure to BTEX in a Municipal Wastewater Treatment Plant in Middle East City: Shiraz, Iran. *Environ. Res.* **2022**, *204*, 112155. [[CrossRef](#)]
15. Almeida, I.L.S.; Filho, N.R.A.; Alves, M.I.R.; Carvalho, B.G.; Coelho, N.M.M. Removal of BTEX from Aqueous Solution Using Moringa Oleifera Seed Cake. *Environ. Technol.* **2012**, *33*, 1299–1305. [[CrossRef](#)]
16. Yahya, A.A.; Rashid, K.T.; Ghadhban, M.Y.; Mousa, N.E.; Majdi, H.S.; Salih, I.K.; Alsahy, Q.F. Removal of 4-Nitrophenol from Aqueous Solution by Using Polyphenylsulfone-Based Blend Membranes: Characterization and Performance. *Membranes* **2021**, *11*, 171. [[CrossRef](#)]
17. Kuntail, J.; Jain, Y.M.; Shukla, M.; Sinha, I. Adsorption Mechanism of Phenol, p-Chlorophenol, and p-Nitrophenol on Magnetite Surface: A Molecular Dynamics Study. *J. Mol. Liq.* **2019**, *288*, 111053. [[CrossRef](#)]
18. Zhou, W.; Ye, Z.; Nikiforov, A.; Chen, J.; Wang, J.; Zhao, L.; Zhang, X. The Influence of Relative Humidity on Double Dielectric Barrier Discharge Plasma for Chlorobenzene Removal. *J. Clean. Prod.* **2021**, *288*, 125502. [[CrossRef](#)]
19. Wan, J.; Chakraborty, T.; Xu, C.; Ray, M.B. Treatment Train for Tailings Pond Water Using Opuntia Ficus-Indica as Coagulant. *Sep. Purif. Technol.* **2019**, *211*, 448–455. [[CrossRef](#)]
20. Kvočka, D.; Žagar, D.; Banovec, P. A Review of River Oil Spill Modeling. *Water* **2021**, *13*, 1620. [[CrossRef](#)]
21. Zhao, C.; Zhou, J.; Yan, Y.; Yang, L.; Xing, G.; Li, H.; Wu, P.; Wang, M.; Zheng, H. Application of Coagulation/Flocculation in Oily Wastewater Treatment: A Review. *Sci. Total Environ.* **2021**, *765*, 142795. [[CrossRef](#)] [[PubMed](#)]
22. Li, B.; Zhao, J.; Ge, W.; Li, W.; Yuan, H. Coagulation-Flocculation Performance and Floc Properties for Microplastics Removal by Magnesium Hydroxide and PAM. *J. Environ. Chem. Eng.* **2022**, *10*, 107263. [[CrossRef](#)]
23. Ferrari, A.M.; Marques, R.G.; de Souza, R.P.; Gimenes, M.L.; Fernandes, N.R.C. Treatment of Wastewater from a Gas Station by Tannin-Based Coagulant and the Sludge Characteristics. *Desalin. Water Treat.* **2020**, *203*, 112–118. [[CrossRef](#)]
24. Zhang, Z.; Du, X.; Carlson, K.H.; Robbins, C.A.; Tong, T. Effective Treatment of Shale Oil and Gas Produced Water by Membrane Distillation Coupled with Precipitative Softening and Walnut Shell Filtration. *Desalination* **2019**, *454*, 82–90. [[CrossRef](#)]
25. Rodriguez, A.Z.; Wang, H.; Hu, L.; Zhang, Y.; Xu, P. Treatment of Produced Water in the Permian Basin for Hydraulic Fracturing: Comparison of Different Coagulation Processes and Innovative Filter Media. *Water* **2020**, *12*, 770. [[CrossRef](#)]
26. Daifa, M.; Shmoeli, E.; Domb, A.J. Enhanced Flocculation Activity of Polyacrylamide-based Flocculant for Purification of Industrial Wastewater. *Polym. Adv. Technol.* **2019**, *30*, 2636–2646. [[CrossRef](#)]
27. Dayarathne, H.N.; Angove, M.J.; Aryal, R.; Abuel-Naga, H.; Mainali, B. Removal of Natural Organic Matter from Source Water: Review on Coagulants, Dual Coagulation, Alternative Coagulants, and Mechanisms. *J. Water Process Eng.* **2021**, *40*, 101820. [[CrossRef](#)]
28. González, T.; Domínguez, J.R.; Beltrán-Heredia, J.; García, H.M.; Sanchez-Lavado, F. Aluminium Sulfate as Coagulant for Highly Polluted Cork Processing Wastewater: Evaluation of Settability Parameters and Design of a Clarifier-Thickener Unit. *J. Hazard. Mater.* **2007**, *148*, 6–14. [[CrossRef](#)]
29. Gingerich, D.B.; Liu, J.; Mauter, M.S. Carbon Benefits of Drinking Water Treatment Electrification. *ACS ES&T Eng.* **2022**, *2*, 367–376. [[CrossRef](#)]
30. Dąbska, A.; Léthel, A. Swelling Behaviours of Compacted Lime-Softening Sludge for Application in Landfill Liners. *Sci. Rep.* **2021**, *11*, 15220. [[CrossRef](#)] [[PubMed](#)]
31. Caron-Beaudoin, É.; Ayotte, P.; Aker, A.; Blanchette, C.; Ricard, S.; Gilbert, V.; Avard, E.; Lemire, M. Exposure to Benzene, Toluene and Polycyclic Aromatic Hydrocarbons in Nunavimmiut Aged 16 Years and over (Nunavik, Canada)—Qanuilirpitaa 2017 Survey. *Environ. Res.* **2022**, *206*, 112586. [[CrossRef](#)] [[PubMed](#)]

32. Putz, G.; Miller, S.; Robertson, J.; Luby, T.; Pernitsky, D.; Edwards, G.; (Stantec Consulting Ltd. Associated Engineering, Saskatoon, SK, Canada). Final Consultant Report Provided by the City of Saskatoon Water Treatment Plant Source Water Resiliency Study. Private Communication, 2018.
33. Agbovi, H.K.; Wilson, L.D.; Tabil, L.G. Biopolymer Flocculants and Oat Hull Biomass To Aid the Removal of Orthophosphate in Wastewater Treatment. *Ind. Eng. Chem. Res.* **2017**, *56*, 37–46. [[CrossRef](#)]
34. Agbovi, H.K.; Wilson, L.D. Optimisation of Orthophosphate and Turbidity Removal Using an Amphoteric Chitosan-Based Flocculant–Ferric Chloride Coagulant System. *Environ. Chem.* **2019**, *16*, 599. [[CrossRef](#)]
35. Abdulhameed, A.S.; Firdaus Hum, N.N.M.; Rangabhashiyam, S.; Jawad, A.H.; Wilson, L.D.; Yaseen, Z.M.; Al-Kahtani, A.A.; ALOthman, Z.A. Statistical Modeling and Mechanistic Pathway for Methylene Blue Dye Removal by High Surface Area and Mesoporous Grass-Based Activated Carbon Using K₂CO₃ Activator. *J. Environ. Chem. Eng.* **2021**, *9*, 105530. [[CrossRef](#)]
36. Kong, D.; Kusriani, E.; Wilson, L.D. Binary Pectin-Chitosan Composites for the Uptake of Lanthanum and Yttrium Species in Aqueous Media. *Micromachines* **2021**, *12*, 478. [[CrossRef](#)]
37. Guo, R.; Bharadwaj, L.; Wilson, L.D. Adsorption Studies of Waterborne Trihalomethanes Using Modified Polysaccharide Adsorbents. *Molecules* **2021**, *26*, 1431. [[CrossRef](#)] [[PubMed](#)]
38. Kong, D.; Wilson, L.D. Uptake of Methylene Blue from Aqueous Solution by Pectin–Chitosan Binary Composites. *J. Compos. Sci.* **2020**, *4*, 95. [[CrossRef](#)]
39. Ahmed, S.; Mustaan, N.; Sheraz, M.A.; un Nabi, S.A.A.; Ahmad, I. Validation of a UV Spectrometric Method for the Assay of Tolfenamic Acid in Organic Solvents. *J. Pharm.* **2015**, *2015*, 216249. [[CrossRef](#)]
40. Wu, Z.; Sun, Z.; Liu, P.; Li, Q.; Yang, R.; Yang, X. Competitive Adsorption of Naphthalene and Phenanthrene on Walnut Shell Based Activated Carbon and the Verification via Theoretical Calculation. *RSC Adv.* **2020**, *10*, 10703–10714. [[CrossRef](#)]
41. Sree, V.G.; Sohn, J.I.; Im, H. Pre-Anodized Graphite Pencil Electrode Coated with a Poly(Thionine) Film for Simultaneous Sensing of 3-Nitrophenol and 4-Nitrophenol in Environmental Water Samples. *Sensors* **2022**, *22*, 1151. [[CrossRef](#)]